Anisotropic elastic-stiffness coefficients of an amorphous Ni–P film

Cite as: Journal of Applied Physics **91**, 4857 (2002); https://doi.org/10.1063/1.1457542
Submitted: 26 October 2001 . Accepted: 11 January 2002 . Published Online: 29 March 2002

Hirotsugu Ogi, Goh Shimoike, Masahiko Hirao, Kazuki Takashima, and Yakichi Higo

Anisotropic elastic-stiffness coefficients of an amorphous Ni–P film

Hirotsugu Ogi,[a] Goh Shimoike, and Masahiko Hirao
Graduate School of Engineering Science, Osaka University, Machikaneyama 1-3, Toyonaka, Osaka 560-8531, Japan

Kazuki Takashima and Yakichi Higo
Precision and Intelligence Laboratory, Tokyo Institute of Technology, Midori-ku, Yokohama, Kanagawa 226-8503, Japan

(Received 26 October 2001; accepted for publication 11 January 2002)

This study presents a complete set of effective elastic-stiffness coefficients of a $Ni_{80}P_{20}$ amorphous-alloy thin film deposited on an aluminum-alloy substrate by electroless plating. The film thickness was 12 μm. The electromagnetic-acoustic-resonance method detected resonance frequencies of the triple-layered specimens (film/substrate/film), which enabled us to determine all five independent elastic-stiffness coefficients of the film using known substrate elastic properties. The resulting coefficients were those of a transverse isotropic material. There was strong anisotropy between the in-plane and normal directions; the in-plane Young's modulus is larger than the normal Young's modulus by 34%, for example. The anisotropic coefficients can be interpreted by considering a micromechanics model for local incomplete cohesion (thin ellipsoidal voids) aligned parallel to the film surface. © *2002 American Institute of Physics.* [DOI: 10.1063/1.1457542]

I. INTRODUCTION

Many thin films appear as candidates for a wide variety of advanced applications such as microelectronics devices, data-storage media, and microelectromechanical systems (MEMS). Among them, amorphous-alloy thin films are suitable for biomedical devices because of their high resistance to corrosion. Understanding their mechanical properties is the key to designing applications and improving the film-processing techniques. In particular, elastic-stiffness coefficients remain issues of central importance because various film-processing techniques produce various elastic stiffnesses. Thus developing a reliable methodology for measuring elastic-stiffness coefficients of thin films is a matter of great interest.

It is considered that such a thin film exhibits anisotropy in the elastic properties between the in-plane (film-plane) and normal (film-growth) directions. In this case, the film shows transverse isotropy (or hexagonal symmetry) and possesses five independent elastic-stiffness coefficients C_{ij} (C_{11}, C_{33}, C_{12}, C_{13}, and C_{44}). Indeed, anisotropic magnetic properties have been reported for amorphous-alloy thin films,[1] indicating elastic anisotropy as well.

Several techniques have been reported for measuring the thin-film C_{ij}. The typical acoustic approach measures the flexural-vibration resonance frequency of a reed composed of a film/substrate layered plate to calculate the in-plane Young's modulus.[2–4] This method always involves ambiguity caused by the mechanical contacts needed for the acoustic transduction and supports. Huang and Spaepen[5] developed a quasistatic uniaxial-tension measurement to obtain the in-plane Young's modulus of free-standing films. They adopted a laser strain measurement to minimize the gripping influence. Another approach is to use surface-acoustic-wave transducers attached to the films to measure the velocities that provide some of the C_{ij}.[6,7] Recently, Brillouin scattering[8] has been used for measuring the Rayleigh-wave velocity traveling along the film surface, which is closely related to the shear modulus polarized perpendicular to the surface (C_{44}). Thus existing methods provide only a few elastic-stiffness coefficients.

In the present study we develop an advanced methodology for measuring the elastic-stiffness tensor of a thin film and apply it to a Ni–P amorphous-alloy film deposited on an Al–Mg-alloy substrate. Free-vibration resonance frequencies of such a layered solid depend on all the film's C_{ij} and the substrate C_{ij} as well as their dimensions and mass densities. Therefore measurements of the resonance frequencies and use of known substrate properties allow one to deduce the film's C_{ij}. However, because of weak contributions of the film C_{ij} to the resonance frequencies, their successful determination requires high accuracy in measuring the resonance frequencies, and any mechanical contact to the specimen should be eliminated or minimized. We achieved this by contactless acoustic excitation and detection with electromagnetic acoustic resonance (EMAR).

Determination of the film's C_{ij} proceeds in two steps. First, we determine C_{33} and C_{44} by measuring the thickness resonance frequencies of the layered plate specimen Ni–P/Al–Mg/Ni–P. Different dependencies of the fundamental and higher resonance modes on the film moduli and density allow their simultaneous determination. Second, we deduce the remaining three stiffnesses by measuring the free-vibration resonance frequencies of a rectangular-parallelepiped specimen and by performing an inverse calculation to find the most suitable C_{ij} to provide the observed resonance frequencies. The resultant C_{ij} showed elastic anisotropy despite Ni–P being an amorphous alloy.

[a]Electronic mail: ogi@me.es.osaka-u.ac.jp

II. MATERIAL

Ni-11.5mass%P($Ni_{80}P_{20}$) amorphous alloy was deposited on both surfaces of polycrystalline Al-4.5mass%Mg plate by electroless plating.[9] The Ni–P film was 12 μm in thickness and the total thickness of the triple-layered specimen (Ni–P/Al–Mg/Ni–P) was 0.799 mm. The thickness-resonance measurement, described below, gave the isotropic substrate stiffnesses as $C_{11}=106.7\pm0.05$ GPa and $C_{44}=26.36\pm0.005$ GPa. Archimedes-method mass density of the substrate was 2645 kg/m^3. Film surface roughness was less than 1 nm. Through-thickness observation of the film by transmission electron microscopy showed no defects and a halo-ring electron diffraction pattern appeared, a typical characteristic of an amorphous phase. We assume transverse isotropy for the film.

We machined three square-cross-section specimens, measuring 30 mm on each side, from a large layered plate for the thickness-resonance measurements; and two rectangular parallelepiped specimens measuring $2.607\times2.599\times0.799$ and $2.679\times2.618\times0.799$ mm^3 for the subsequent free-vibration-resonance measurements.

Throughout this study we use a coordinate system where the x_1-x_2 plane is parallel to the film surface and the x_3 axis is along the normal direction. We made all measurements in a heat- insulated chamber, which regulates the specimen temperature to 30 ± 0.05 °C.

III. ELECTROMAGNETIC ACOUSTIC RESONANCE

A. Thickness resonance of layered plate

We derive the frequency equation for a triple-layered plate by considering six partial plane waves traveling along the x_3 direction. The resulting expression takes the form (see Appendix A)

$$C_f k_f \tan\eta = C_s k_s \frac{\cos\gamma\sin\delta-\sin\gamma\cos\delta}{\cos\gamma\cos\delta+\sin\gamma\sin\delta}, \tag{1}$$

where

$$\cos\delta=\cos\alpha\cos\beta+\kappa\sin\alpha\sin\beta,$$

$$\sin\delta=\cos\alpha\sin\beta-\kappa\sin\alpha\cos\beta, \tag{2}$$

and

$$\alpha=k_f d_1,\quad \beta=k_s d_1,\quad \gamma=k_s(d_1+d_2),\quad \eta=k_f d_3,$$

and

$$\kappa=\frac{C_f k_f}{C_s k_s}. \tag{3}$$

C_f and C_s denote the film and substrate elastic constants, respectively, either for the longitudinal mode (C_{33}) or shear mode (C_{44}). k_f and k_s denote the wave numbers for the film and substrate, respectively, and they are expressed by the wave velocity v and the resonance frequency f as $k=2\pi f/v$. d_1 and d_3 denote the film thicknesses and d_2 the substrate thickness. Equation (1) applies also to a double-layered specimen (film/substrate) by taking $d_3=0$.

We used a bulk-wave electromagnetic acoustic transducer (EMAT).[10,11] It consists of a spiral-elongated coil and a pair of permanent magnets mounting the coil to generate and detect the longitudinal wave and the shear wave polarized parallel to the film surface, relying on the Lorentz-force mechanism. The EMAT proving area was 5×7 mm^2. We excited the EMAT with long tone bursts to launch the bulk waves into the thickness direction. After the excitation, we detected the reverberating signal by the same EMAT and processed it with a superheterodyne spectrometer to extract the signal amplitude of the same frequency component as the driving bursts. A frequency scan gives a resonance spectrum as shown in Fig. 1.

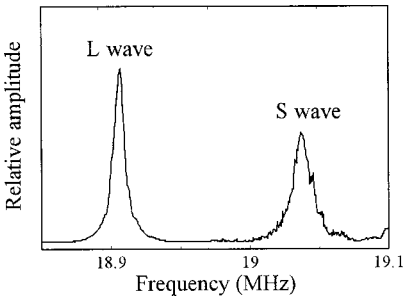

FIG. 1. Thickness-resonance spectrum measured for the Ni–P/Al–Mg/Ni–P triple-layered plate. The fifth longitudinal-wave resonance peak and the tenth shear-wave resonance peak appear.

For determining accurate substrate C_{ij}, we measured the resonance frequencies of the substrate plate alone; after finishing the measurements for the film/substrate/film plate we removed the film layers. We then deduced the film's C_{33}, C_{44}, and density from Eq. (1) using the measured resonance frequencies of both the multilayer specimen and the substrate as well as their thicknesses.

B. Free-vibration resonance of a layered rectangular parallelepiped

We derived the remaining three stiffnesses (C_{11}, C_{12}, and C_{13}) by resonance ultrasound spectroscopy (RUS).[12–16] Basically, this method is capable of finding complete sets of elastic-stiffness coefficients of bulk anisotropic solids with higher accuracy than other methods. It involves measurement of the free-vibration resonance frequencies of the solid and an inverse calculation to find a set of C_{ij} that provides the closest resonance frequencies to the measurements. The inverse calculation requires Lagrangean minimization with the Rayleigh–Ritz approach for calculating the resonance frequencies and a least-squares fitting between the measurements and calculations.

Because no analytical solution exists for a rectangular-parallelepiped solid, the displacements in the vibrating solid have been approximated by linear combinations of the normalized Legendre functions[12] or simply of the power series.[13] For a layered rectangular parallelepiped, however, such a basis function fails to express the strain discontinuity at the interfaces caused by the different elastic moduli. Heyliger,[17] therefore, separated the x_1-x_2 and x_3 dependences of the displacements. He used a power series ($x_1^k x_2^l$, k, $l=0,1,2,...$) for the x_1-x_2 dependence and Lagrangean

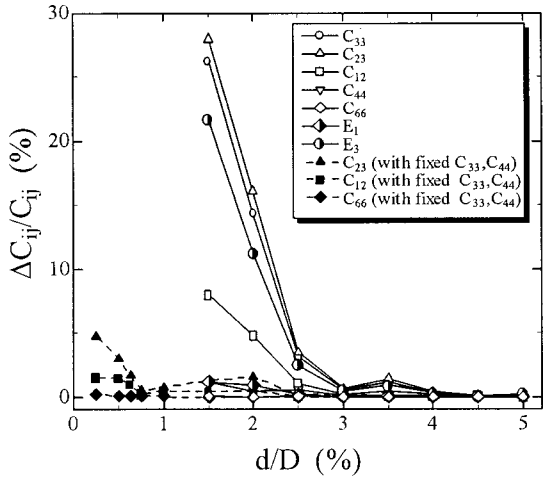

FIG. 2. Errors of inversely deduced monocrystal titanium-film C_{ij} with various film thicknesses. The same material was assumed for the substrate.

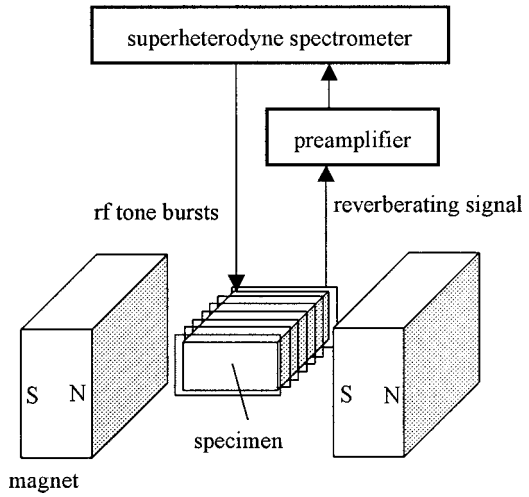

FIG. 3. Measurement setup of the mode-selective resonance ultrasound spectroscopy.

interpolation polynomials for the x_3 dependence. For the displacement along the x_1 axis, the expression is

$$u_1(x_1,x_2,x_3,t)=\sum_{i=1}^{m}\sum_{j=1}^{n} U_{ji}(t)\Psi_i(x_1,x_2)\overline{\Psi}_j(x_3). \quad (4)$$

Here, n denotes the number of layers and m the number of the in-plane basis functions $\Psi_i(x_1,x_2)$. $\overline{\Psi}_j(x_3)$ denotes the one-dimensional Lagrangean interpolation polynomials.[18] Approximations for u_2 and u_3 take similar forms. We followed Heyliger's calculation and used a standard least-squares procedure to inversely deduce the film's C_{ij}.

To study the reliability of the present inverse calculation method we made a numerical simulation of a titanium thin film epitaxially deposited on the (0001) surface of a monocrystal titanium rectangular parallelepiped. The substrate titanium measures $5\times4\times2$ mm^3 and the x_3 axis (c axis) is along the 2-mm side. We used $C_{11}=160$ GPa, $C_{33}=181$ GPa, $C_{13}=66$ GPa, $C_{12}=90$ GPa, $C_{44}=46.5$ GPa, and $\rho=4500$ kg/m^3. The deposition was expressed by an increase of the thickness along the x_3 axis. Because the resultant layered rectangular-parallelepiped Ti/Ti is the same as a homogeneous Ti monocrystal, its free-vibration resonance frequencies can be calculated by the usual method.[12] We regarded them as measurements. Then, assuming that a surface layer of unknown material had been deposited, we deduced the film C_{ij} by the inverse-calculation procedure based on Heyliger's approach using the known substrate C_{ij} and density, the film thickness and density, and the *measured* resonance frequencies. The converged film C_{ij} must agree with the substrate C_{ij} because the same material was added. We investigated this agreement with various film thicknesses.

Figure 2 shows the result, where D is the substrate thickness (2 mm) and d the film thickness. We could deduce the film C_{66} and the in-plane Young's modulus E_1 within 1.5% error for $d/D\geqslant1.5\%$, while the converged C_{33}, C_{12}, C_{13}, and the normal Young's modulus E_3 contained large errors for $d/D<2.5\%$. In the free vibration of the rectangular- parallelepiped solid, many flexural and torsional vibrations appear, which cause maximum bending and shearing stresses at the specimen surfaces where the film is deposited. The film E_1 and C_{66} can, therefore, contribute a lot to those vibration modes. However, other elastic constants contribute little. For example, C_{33} affects mostly the longitudinal-mode wave that propagates in the thickness direction and such a C_{33}-dependent mode appears at much higher frequencies, where a large number of overlapping overtone peaks occur from other vibration modes to overlap it. Thus the free-vibration-resonance method provides accurate C_{66} and E_1, but inaccurate other C_{ij}. For this reason we separately determined C_{33} and C_{44} using the thickness-resonance method. Indeed, when C_{33} and C_{44} are fixed, the remaining three elastic constants are determined within 5% error for $d/D>0.2\%$ (see Fig. 2).

The thickness ratio d/D of the Ni–P/Al–Mg/Ni–P specimen equals 1.54%, suggesting that a reliable set of C_{ij} of the Ni–P film can be obtained by the combination of the two resonance methods.

Exact mode identification is essential for the least-squares fitting between the measured and calculated resonance frequencies. However, this is not an easy task in the conventional RUS method because too many resonance modes are simultaneously excited, causing peak overlapping. We overcame this difficulty by selecting one vibration group by controlling the Lorentz-force direction. (There are four vibration groups for a layered rectangular parallelepiped according to the deformation symmetry, as tabulated by Heyliger.[17]) Figure 3 shows the typical measurement setup with EMAR. We inserted the specimen in the solenoid coil and located a pair of permanent magnets outside the coil to provide the static-magnetic field for the electromagnetic excitation and detection of free vibration. The field direction was changeable to control the Lorentz-force direction and then to select a vibration group. The mode-selective principle is discussed in detail in Ref. 19.

IV. RESULTS

A. C_{33} and C_{44}

Using Eq. (1), we calculated the dependencies of the thickness resonance frequencies on the film's shear modulus

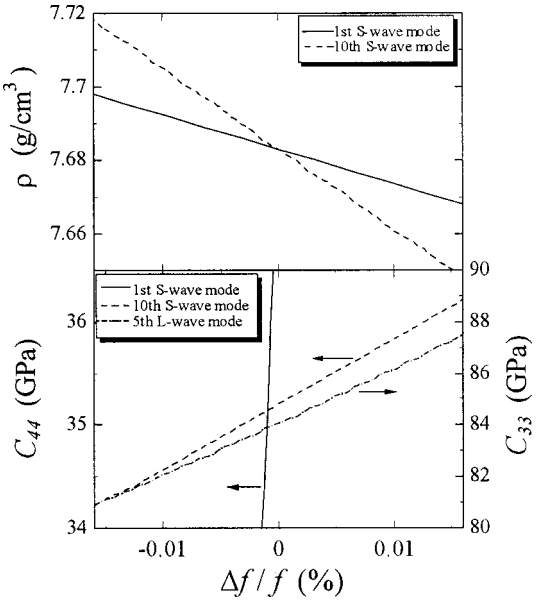

FIG. 4. Dependences of the thickness-resonance frequencies on the moduli and density of the Ni–P film.

TABLE I. Elastic-stiffness coefficients (GPa) and density of Ni–P amorphous-alloy thin films. The film-growth direction is along the x_3 direction.

	Present $Ni_{80}P_{20}$ (film)	Micromechanics prediction	Reference 20 $Ni_{76}P_{24}$ (film)	Reference 21 $Ni_{76}P_{24}$ (film)
C_{11}	140±14	139		
C_{33}	85±3.0	86		
C_{12}	64±14	63		
C_{13}	30±15	45		
C_{44}	35.2±0.8	31		
C_{66}[a]	38.3±0.5	38		35
E_1	107±1.0	102	100	95
E_3	76±8.0	66		
B	65±1.5	71		111
ν_{12}	0.41±0.015	0.34		0.36
ν_{13}	0.21±0.1	0.34		
ν_{31}	0.14±0.05	0.22		
ρ (g/cm³)	7.68±0.015		7.86	7.79

[a]$C_{66}=(C_{11}-C_{12})/2$.

(C_{44}), longitudinal-wave modulus (C_{33}), and density ρ (Fig. 4). The film C_{44} least affects the fundamental resonance frequency because of nearly uniform displacement and then nearly zero shear stress within the film. The sensitivity of the resonance frequency to the film's moduli increases with the resonance order. On the other hand, the density most affects the fundamental mode because of the largest particle acceleration and inertia resistance at the film, which is sensitive to the film mass. Thus we used the fundamental shear-wave resonance to determine the film density and the higher-order modes shown in Fig. 1 for the film's C_{44} and C_{33}. Reproducibility of a single resonance-frequency measurement was on the order of 10^{-6}. The standard deviation among completely independent measurements was less than 0.005%. The results are given in Table I with the possible maximum errors, which contain the standard deviation and differences among the three specimens.

B. C_{11}, C_{12}, and C_{13}

Figure 5 shows the free-vibration resonance spectra of the rectangular-parallelepiped specimen, demonstrating that each vibration group is independently excited. The reproducibility of the measurements was of the same order as the thickness-resonance measurements. Table II compares the measurements with the calculations after the inverse calculation. Typical rms difference between them was 0.2%, which was one-order smaller than the C_{ij} contribution to the resonance frequencies [i.e., $(C_{ij}/f)(\partial f/\partial C_{ij})$]. The resulting three C_{ij} are given in Table I with the possible maximum errors, which contain the measurement difference between the two specimens.

V. DISCUSSION

In Table I we compare the present results with those reported for Ni–P amorphous-alloy thin films in the past. Barmatz and Chen[20] used a vibrating-reed method for the in-plane Young's modulus (E_1), and Logan and Ashby[21] used tension and torsion measurements for E_1 and the in-plane shear modulus (C_{66}). Their results are comparable with our E_1 and C_{66} despite a slight difference of chemical composition. The Logan–Ashby bulk modulus B disagrees with ours because they assumed that the material is isotropic.

Concerning Ni–P amorphous-alloy film, this is the first report of the complete set of elastic-stiffness coefficients with transverse isotropy. Particularly significant is elastic anisotropy between in- plane and out-of-plane directions; C_{11} is larger than C_{33} by 49%, E_1 larger than E_3 by 34%, and C_{66} larger than C_{44} by 8.4%. For the same material, Takashima *et al.*[22,23] observed strong anisotropy in the crack-growth behavior. The fracture-toughness values were 4.2 and 7.3 MPa $m^{1/2}$ for cracks propagating in the in-plane and out-

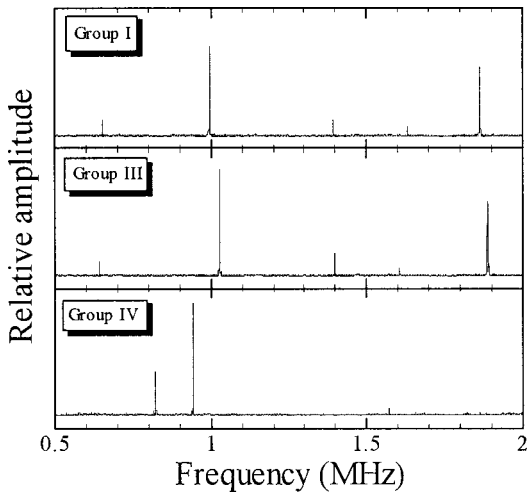

FIG. 5. Resonance spectra of the free vibration of the Ni–P/Al–Mg/Ni–P layered rectangular parallelepiped specimen, measuring 2.679×2.618 ×0.799 mm^3. Individual measurement setup excites one vibration group among four groups.

TABLE II. Measured resonance frequencies (f_{meas}) and calculated resonance frequencies f_{calc} for the Ni–P/Al–Mg/Ni–P rectangular parallelepiped specimen, measuring $2.679\times2.618\times0.799$ mm^3. The rms difference between them is 0.2%.

Group	f_{meas} (MHz)	f_{calc} (MHz)	diff (%)
I	0.650 458	0.649 062	−0.21
	0.994 308	0.994 861	0.06
	1.392 840	1.395 308	0.18
	1.631 315	1.632 315	0.06
	1.864 601	1.865 514	0.05
III	0.641 412	0.640 453	−0.15
	1.027 070	1.023 561	−0.34
	1.396 996	1.397 333	0.02
	1.604 992	1.608 280	0.20
	1.892 098	1.882 969	−0.48
IV	0.819 586	0.819 504	−0.01
	0.940 220	0.942 139	0.20
		1.101 383	
	1.571 404	1.575 227	0.24

of-plane directions, respectively, indicating that this material is more tolerant to crack propagation in the film-growth direction. Our larger C_{11} suggests stronger in-plane binding force, consistent with their observation.

There are two possible mechanisms for the elastic anisotropy in the amorphous-alloy film. First is inhomogeneous microstructure. Phosphorus-rich and phosphorus-poor regions could appear periodically to make the columnar structure as actually seen in Fe–P amorphous-alloy film.[24] Also, chemical composition could vary in the film-growth direction. Both inhomogeneities may cause transverse isotropy. Second is local incomplete cohesion inside the film material,[5] which would occur during deposition. Incomplete cohesive regions lying in the x_1-x_2 plane will cause transverse-isotropic effective stiffnesses. Considering the strong anisotropy observed here, it is more likely that the latter dominates. We estimate this effect using a micromechanics model by replacing the incomplete cohesive regions with oblate ellipsoidal microcracks aligned parallel to the depositing face. As shown in Appendix B, this model reconstructed the effective elastic-stiffness coefficients close to the measurements with a very small volume fraction (5×10^{-5}) and an aspect ratio $a_3/a_1=10^{-4}$ of the inclusion. Thus aligned microcracking can cause such a strong anisotropy even with an isotropic matrix. It is difficult to observe the incomplete cohesive region with microscopic observations and their presence remains better than hypothetical at present. Such a structural inhomogeneity may occur in many thin films and elastic-anisotropy measurement may provide a significant means for evaluating the thin-film microstructures.

VI. CONCLUSIONS

We proposed a contactless method relying on electromagnetic acoustic resonance for determining all the elastic-stiffness coefficients of anisotropic thin films. We derived a frequency equation for the thickness resonance in a triple-layered plate, and we developed an inverse calculation for the layered rectangular-parallelepiped specimen by incorporating the linear Lagrangean-interpolation polynomials in the basis functions. The EMAR method determined the resonance frequencies with reproducibility better than 10^{-5}, which allowed us to evaluate the film elastic-stiffness coefficients within 5% error when the film-to-substrate thickness ratio is larger than 0.2%.

Assuming transverse isotropy, we presented a complete set of elastic-stiffness coefficients of Ni–P amorphous-alloy thin film deposited on an Al–Mg substrate. The most important observation is the strong elastic anisotropy between in-plane and out-of-plane directions. On the basis of a micromechanics calculation, thin microcracks aligned parallel to the film surface could explain the anisotropy.

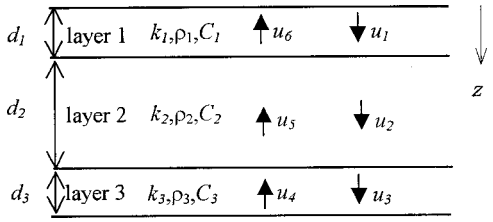

FIG. 6. Six partial plane waves (longitudinal wave or shear wave) traveling in the triple-layered plate in the thickness (z) direction. ρ_j denotes density of the j layer.

APPENDIX A

We consider six partial plane waves, either longitudinal waves or shear waves polarized parallel to the surface, traveling in the thickness direction z of a triple-layered plate (Fig. 6):

$$u_1=U_1e^{j(\omega t-k_1z)},\quad u_2=U_2e^{j(\omega t-k_2z+\phi_2)},$$
$$u_3=U_3e^{j(\omega t-k_3z+\phi_3)},\quad u_4=U_4e^{j(\omega t+k_3z+\phi_4)},$$
$$u_5=U_3e^{j(\omega t+k_2z+\phi_5)},\quad u_6=U_6e^{j(\omega t+k_1z+\phi_6)}. \tag{A1}$$

Here, U_i and ϕ_i denote the amplitude and phase of the ith partial wave. ω denotes the angular frequency and d_j the thickness of the jth layer. k_j denotes the wave number in the jth phase, that is, $k_j=\omega/v_j$ (v_j is the longitudinal-wave or shear-wave velocity). There are four boundaries, two free boundaries and two interfaces between the layers. The stress-free boundary conditions at $z=0$ and $z=d_1+d_2+d_3$ are

$$C_1\frac{\partial}{\partial z}(u_1+u_6)=0,\quad \text{and}\quad C_3\frac{\partial}{\partial z}(u_3+u_4)=0, \tag{A2}$$

respectively. At the layer interfaces, continuity of displacements and stresses is required:

$$u_1+u_6=u_2+u_5$$

and

$$C_1\frac{\partial}{\partial z}(u_1+u_6)=C_2\frac{\partial}{\partial z}(u_2+u_5),\quad \text{at } z=d_1, \tag{A3}$$

and

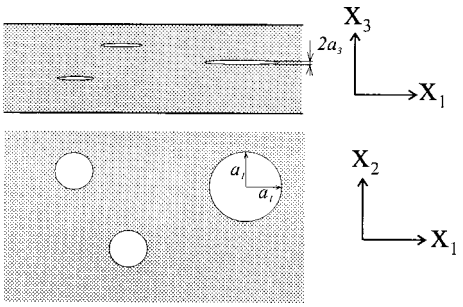

FIG. 7. Oblate ellipsoidal microcracks for modeling the incomplete-cohesion regions within the film.

$$u_2+u_5=u_3+u_4$$

and

$$C_2\frac{\partial}{\partial z}(u_2+u_5)=C_3\frac{\partial}{\partial z}(u_3+u_4)$$

$$\text{at}\quad z=d_1+d_2. \tag{A4}$$

Here, C_i denotes the longitudinal or shear modulus of the i layer. Substitution of Eq. (A1) into Eqs. (A2)–(A4) results in the frequency equation for the through-thickness resonance of the triple-layered plate:

$$C_3k_3\tan\eta-C_2k_2\frac{\{\cos\gamma\sin\delta-\sin\gamma\cos\delta\}}{\{\cos\gamma\cos\delta+\sin\gamma\sin\delta\}}=0, \tag{A5}$$

Here,

$$\cos\delta=\cos\alpha\cos\beta+\kappa\sin\alpha\sin\beta,$$

$$\sin\delta=\cos\alpha\sin\beta-\kappa\sin\alpha\cos\beta, \tag{A6}$$

and

$$\alpha=k_1d_1,\quad \beta=k_2d_1,\quad \gamma=k_2(d_1+d_2),$$

$$\eta=k_3d_3,\quad \kappa=\frac{C_1k_1}{C_2k_2}. \tag{A7}$$

In the present study, $C_1=C_3=C_f$, $C_2=C_s$, $k_1=k_3=k_f$, and $k_2=k_s$.

APPENDIX B

We consider the Ni–P amorphous alloy to contain aligned oblate ellipsoidal microcracks with two equal major axes in the film plane (a_1) and the third major axis along the film-thickness direction (a_3) as illustrated in Fig. 7. We assume isotropic symmetry for the amorphous-alloy matrix.

The effective elastic stiffness of the dual-phase composite **C** can be expressed with strain concentration factor **A**:[25]

$$\mathbf{C}=\mathbf{C}_M+f(\mathbf{C}_I-\mathbf{C}_M)\mathbf{A}. \tag{B1}$$

Here, $\mathbf{C}_M$ and $\mathbf{C}_I$ denote the elastic-stiffness tensors of the matrix amorphous alloy and the microcracks (inclusions). f denotes the volume fraction of the microcracks. **A** is given by the Mori–Tanaka mean-field theory[26] as

$$\mathbf{A}=\mathbf{A}_D[(1-f)\mathbf{I}+f\mathbf{A}_D]^{-1},$$

$$\mathbf{A}_D=[\mathbf{I}+\mathbf{S}\mathbf{C}_M^{-1}(\mathbf{C}_I-\mathbf{C}_M)]^{-1}. \tag{B2}$$

Equation (B2) is derived analytically using Eshelby's equivalent-inclusion method.[27] The effect of the microcrack shape is contained in the Eshelby tensor **S**, which is a function of Poisson's ratio ν of the isotropic matrix. For the microcracks shape considered here, the nonzero components of **S** are

$$S_{11}=S_{22}=\frac{\pi(13-8\nu)}{32(1-\nu)}\frac{a_3}{a_1},\quad S_{33}=1-\frac{\pi(1-2\nu)}{4(1-\nu)}\frac{a_3}{a_1},$$

$$S_{12}=S_{21}=-\frac{\pi(1-8\nu)}{32(1-\nu)}\frac{a_3}{a_1},$$

$$S_{31}=S_{32}=\frac{\nu}{1-\nu}\left\{1-\frac{\pi(1+4\nu)}{8\nu}\frac{a_3}{a_1}\right\},$$

$$S_{44}=S_{55}=1-\frac{\pi(2-\nu)}{4(1-\nu)}\frac{a_3}{a_1},\quad S_{66}=\frac{\pi(7-8\nu)}{16(1-\nu)}\frac{a_3}{a_1}. \tag{B3}$$

Arbitrarily taking $C_{M11}=160$ GPa, $C_{M44}=38$ GPa, $\mathbf{C}_I=\mathbf{0}$, $a_3/a_1=10^{-4}$, and $f=5\times10^{-5}$, we obtained the effective modulus **C** as given in Table I.

[1] B. Lanchava, H. Hoffmann, A. Bechert, S. Gegenfurtner, C. Amann, and I. Rohrmann, J. Magn. Magn. Mater. **176**, 139 (1997).
[2] S. Peraud, S. Pautrot, P. Villechaise, P. Mazot, and J. Mendez, Thin Solid Films **292**, 55 (1997).
[3] S. Sakai, H. Tanimoto, and H. Mizubayashi, Acta Mater. **47**, 211 (1999).
[4] V. D. Papachristos, C. N. Panagopoulos, L. W. Christoffersen, and A. Markaki, Thin Solid Films **396**, 173 (2001).
[5] H. Huang and F. Spaepen, Acta Mater. **48**, 3261 (2000).
[6] A. Moreau, J. B. Ketterson, and J. Huang, Mater. Sci. Eng., A **126**, 149 (1990).
[7] J. O. Kim, J. D. Achenbach, M. Shinn, and S. Barnett, J. Mater. Res. **7**, 2248 (1992).
[8] B. Davis, D. Seidman, A. Moreau, J. Ketterson, J. Mattson, and M. Grimsditch, Phys. Rev. B **43**, 9304 (1991).
[9] H. Li, H. Chen, S. Dong, J. Yang, and J. Deng, Appl. Surf. Sci. **125**, 115 (1998).
[10] M. Hirao, H. Ogi, and H. Fukuoka, Rev. Sci. Instrum. **64**, 3198 (1993).
[11] H. Ogi, J. Appl. Phys. **82**, 3940 (1997).
[12] I. Ohno, J. Phys. Earth **24**, 355 (1976).
[13] A. Migliori and J. Sarrao, *Resonant Ultrasound Spectroscopy* (Wiley, New York, 1997).
[14] H. Ogi, H. Ledbetter, S. Kim, and M. Hirao, J. Acoust. Soc. Am. **106**, 660 (1999).
[15] H. Ogi, K. Takashima, H. Ledbetter, M. L. Dunn, G. Shimoike, M. Hirao, and P. Bowen, Acta Mater. **47**, 2787 (1999).
[16] H. Ogi, M. Dunn, K. Takashima, and H. Ledbetter, J. Appl. Phys. **87**, 2769 (2000).
[17] P. R. Heyliger, J. Acoust. Soc. Am. **107**, 1235 (2000).
[18] J. N. Reddy, Commun. Appl. Numer. Methods **3**, 173 (1987).
[19] H. Ogi, P. Heyliger, H. Ledbetter, and S. Kim, J. Acoust. Soc. Am. **108**, 2829 (2000).
[20] M. Barmatz and H. S. Chen, Phys. Rev. B **9**, 4073 (1974).
[21] J. Logan and M. F. Ashby, Acta Metall. **22**, 1047 (1974).
[22] K. Takashima, A. Ogura, Y. Ichikawa, and Y. Higo, Mater. Res. Soc. Symp. Proc. **657**, EE5.12.1-12.10 (2000).
[23] K. Takashima, M. Shimojo, Y. Higo, and M. V. Swain, in Mechanical Properties of Structural Films, ASTM STP-1413, edited by C. Muhlstein and S. Brown, 2001, p. 72.
[24] S. Armyanov, S. Vitkova, and O. Blajiev, J. Appl. Electrochem. **27**, 185 (1997).
[25] M. L. Dunn and H. Ledbetter, J. Appl. Mech. **62**, 1023 (1995).
[26] T. Mori and K. Tanaka, Acta Metall. **21**, 571 (1973).
[27] T. Mura, *Micromechanics of Defects in Solids*, 2nd ed. (Martinus Nijhoff, The Hague, 1987), p. 394.